

Spectral and polarization modulation of quantum dot emission in a one-dimensional liquid crystal photonic cavity

A. L. Rodarte, C. Gray, L. S. Hirst,^{*} and S. Ghosh[†]*School of Natural Sciences, University of California, Merced, California 95343, USA*

(Received 26 September 2011; revised manuscript received 21 November 2011; published 19 January 2012)

We demonstrate spectral and polarization modulation of chemically synthesized core-shell CdSe/ZnS quantum dots (QDs) embedded in a one-dimensional photonic cavity formed by a cholesteric liquid crystal (CLC) matrix. A Cano-wedge cell varies the pitch of the CLC leading to the formation of Grandjean steps. This spatially tunes the photonic stop band, changing the resonance condition and continuously altering both the emission wavelength and polarization state of the QD ensemble. Using high resolution spatially and spectrally resolved photoluminescence measurements, we find that the emission is elliptically polarized and that the tilt of the ellipse, while dependent on the emission wavelength, additionally varies with distance across the Grandjean steps. This work opens up the possibility of designing new QD based optical devices, such as tunable single photon sources, where spatial control of wavelength and polarization of the embedded QDs would allow great flexibility and added functionalities.

DOI: [10.1103/PhysRevB.85.035430](https://doi.org/10.1103/PhysRevB.85.035430)

PACS number(s): 73.21.La, 78.55.-m, 78.67.-n

I. INTRODUCTION

In recent years there has been increasing interest in research at the interface of hard and soft condensed matter. Soft materials, by definition, are easily modified by external forces, such as those exerted by relatively weak electric or magnetic fields. Therefore, they can provide a reconfigurable medium in which nanoscale structures can be assembled and manipulated. One particularly rich area for investigation in this field is the interaction between dispersed particles and liquid crystal (LC) materials.¹ Liquid crystals are complex fluids in which the constituent molecules have orientational and short-range positional order. A large number of distinct LC phases have been observed and the phase exhibited by a specific material depends on several factors, including molecular structure, temperature, or concentration in a solvent. The well-known thermotropic nematic and cholesteric phases have found wide commercial applicability in display technologies and optical modulation devices. One of the key properties of LC materials is their optical anisotropy, which causes them to be birefringent, which can then be tuned by the application of an external electric field. LC materials can also be confined in a device to produce macroscopic ordered domains with a defined optical axis. This combination of molecular switchability and orientational control offers the potential for novel device geometries with highly tunable optical properties.

Dispersions of a variety of particle geometries such as spherical colloids,²⁻⁴ carbon nanotubes,^{5,6} clay platelets,^{7,8} and other anisotropic morphologies^{9,10} have produced some fascinating results regarding the interplay between particle shape and alignment in the LC phase. Several studies have additionally shown that various LC phases can be used as a template for directed nanoparticle assembly^{11,12} and that the electro-optic response of the LC can be influenced by the addition of nanoparticles.^{13,14} In addition, nanoparticles and colloids have been utilized to control and stabilize topological defects in the anisotropic phase.¹⁵ Recently, stabilization of the LC blue phase over a broad temperature range was achieved using gold nanoparticles localized to the defect cores.¹⁶ While the effects of nanoparticles on an LC host phase have been

studied, less is known about how the LC medium affects the properties of the dispersed nanoparticles, and whether it is possible to use LC materials to achieve new types of directed nanoscale assemblies that would manifest novel functionality.

II. EXPERIMENTAL DETAILS

In this paper, we focus on using the optical activity of an LC host material to influence the photoluminescence (PL) from embedded semiconducting quantum dots (QDs).¹⁷ Light-matter interactions in confined geometries can result in a wide range of applications, such as optical communications,¹⁸ quantum information processing,¹⁹ and quantum computation schemes.²⁰ The cholesteric LC phase, composed of rodlike chiral molecules, can be tailored to give rise to such a confined optical system. Similar to the nematic phase, the cholesteric phase has short-range orientational order defined by the LC director but with the additional feature that the director rotates through the bulk material [Fig 1(a)].²¹ The periodicity of this arrangement results in an alternating modulation of the refractive index, creating a one-dimensional photonic band-gap material. The distance required for the director axis to complete a full rotation is called the pitch (p) and it determines the spectral stop band (reflection band) of the cholesteric liquid crystal (CLC). In typical materials with a stop band, all incident light with wavelengths within the band is preferentially reflected. In CLCs, the chiral geometry adds a special flavor. Even within the stop band only circularly polarized light that has the same handedness as the CLC helix is selectively reflected. Light polarized with the opposite handedness and light with wavelengths outside the stop band are both transmitted through the CLC film.^{22,23} A general case is illustrated in Fig. 1(a) where linearly polarized incident light spectrally matched to the stop band is partly reflected and partly transmitted (as any linear polarization is a sum of right and left circular polarizations). An added attraction of the CLC photonic structure is that it can be modified *in situ* by varying the temperature or applying an electric field,

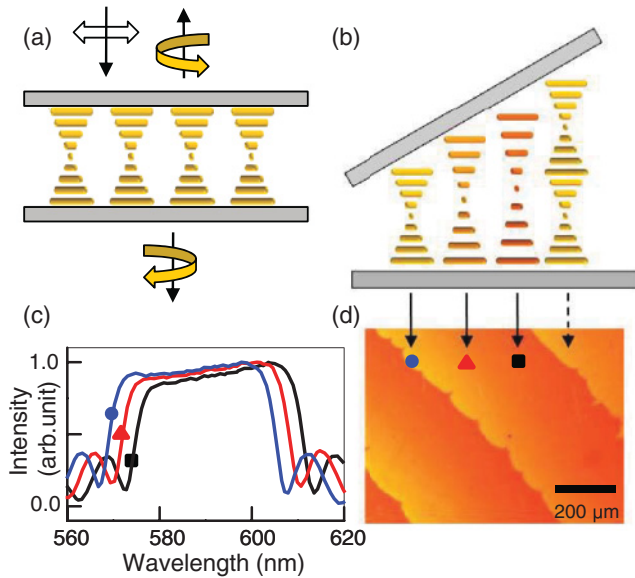


FIG. 1. (Color online) (a) Schematic demonstrating the helical arrangement of the CLC between parallel glass slides. This device geometry selectively reflects and transmits different circular components of linearly polarized incident light. (b) The CLC in a Cano-wedge cell. (c) The spectral stop band (reflection band) of the CLC in the cell at three different points across a single Grandjean step demonstrating the shift of the stop band. (d) Polarized optical microscopy transmission image of the CLC in (b) showing the Grandjean steps. The symbols denote the corresponding stop bands of (c) and the arrows show the corresponding pitch.

thereby allowing spectral tuning of its optical properties and confinement parameters.

If, instead of enclosing the CLC between parallel surfaces, a wedge-shaped arrangement is used, the pitch can be varied across the film, as shown in Fig. 1(b). Commonly known as a Cano-wedge cell,^{24,25} in this device the CLC fills a glass cell where the inside surfaces have been treated with a rubbed planar alignment layer, polyvinylalcohol (PVA, Sigma Aldrich). Because the LC molecules at the surface are constrained by this alignment layer, the helix stretches as more space is available, elongating the pitch continuously by an amount Δs . When $\Delta s = p/2$, there is a discontinuity as the system relaxes to the initial pitch p but with an added extra half turn [dashed arrow in Fig. 1(b)], before the stretching repeats again. The spectral effects of the changing pitch are shown in Figs. 1(c) and 1(d). In Fig. 1(c), as the pitch increases the corresponding stop band is observed to red-shift. When the cell is viewed between crossed polarizers the CLC texture shows the well-known Grandjean steps in Fig. 1(d). The colors observed from a device placed between crossed polarizers are dependent on the pitch of the material and, in our case, a color variation from yellow to orange is seen across each step. The corresponding spatial positions of the stop bands in Fig. 1(c) in the Grandjean step of Fig. 1(d) are marked using symbols.

For our CLC samples we used mixtures of a chiral LC, cholesteryl oleyl carbonate (COC, Sigma Aldrich), and a nematic LC, 4'-penty1/4-biphenylcarbonitrile (5CB, Sigma Aldrich). The initial (unstretched) pitch of the CLC depends on the relative concentrations of the chiral component in the

nematic material. For the sample shown in Fig. 1(d), a mixture of 60 wt% COC to 40 wt% 5CB was prepared by heated bath sonication. The bath was maintained at a temperature above the isotropic transition temperature for both COC and 5CB (38°C and 36°C, respectively) and the sample sonicated for approximately 1 h to ensure complete mixing. To determine the pitch of the material, the mixture was filled between parallel glass plates coated with a rubbed poly-vinyl alcohol (PVA) alignment layer to induce planar alignment of the molecules. The stop band was measured using a Perkin Elmer UV-VIS absorption spectrophotometer. For this sample the pitch was observed to be approximately 590 nm at the center of the stop band [curve marked with solid circle in Fig. 1(c)]. After preparation of the desired cholesteric material, CdSe/ZnS core-shell QDs (N-N Labs, emission peak at 609 nm) were added at a concentration of 0.2 mg/ml and the mixture was sonicated for an additional 3 h at the same elevated temperature. The final mixture was then filled into a Cano-wedge cell at 50°C before cooling on a controlled heating stage (Linkam LTS350) at a rate of 1°C/min to room temperature. On verifying the presence of the Grandjean steps using polarized optical microscopy, spectroscopic measurements were carried out using a custom-made diffraction-limited scanning confocal microscope with an optical resolution of 600 nm and a continuous-wave 532-nm diode laser as the excitation source. The QD PL was collected by an Acton 300i spectrometer and dispersed onto a thermoelectrically cooled CCD (spectral resolution ~ 0.18 nm). By raster scanning selected regions of the sample, spatially resolved PL maps were created to monitor the variation of both emission intensity and wavelength with position.

III. RESULTS AND DISCUSSION

Figure 2 shows three spatially resolved maps of the peak wavelength (λ_{PEAK}) of QD emission measured across a region of the sample that demonstrated clear Grandjean steps when imaged using polarized optical microscopy. In Fig. 2(a) λ_{PEAK} varies across the sample following the Grandjean step pattern closely. The difference in λ_{PEAK} from the beginning (marked “L”) to the end (marked “R”) of a step is approximately 7 nm, increasing from left to right. The sample is then heated past the isotropic transition temperature (to 43°C) and the scan repeated [Fig. 2(b)]. Now we observe that the prior systematic wavelength gradient is replaced by a random

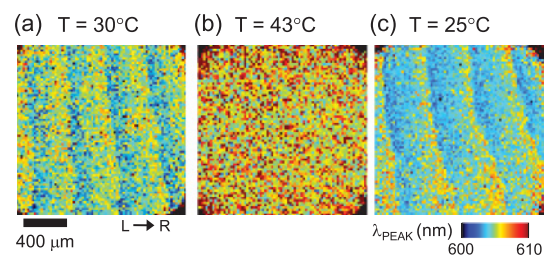


FIG. 2. (Color online) Spatially resolved PL scans of QD-CLC mixture at (a) 35°C, (b) heated to 43°C, and (c) cooled back to 25°C, mapping the emission λ_{PEAK} . L denotes the left edge of a Grandjean step where the pitch is at the minimum value within the step and R denotes the right where the pitch is at the maximum.

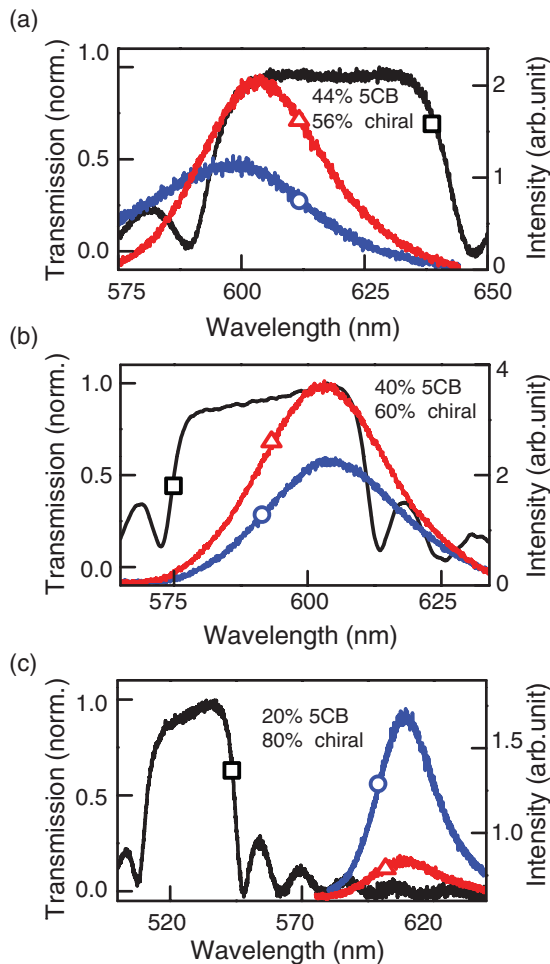


FIG. 3. (Color online) Emission spectra of the QD-CLC mixture in the cholesteric (triangle) and isotropic phases (circle) superimposed on the corresponding stop bands (square) for (a) 44% nematic and 56% chiral LC, (b) 40% nematic and 60% chiral LC, and (c) 20% nematic and 80% chiral LC. Proportions are by weight.

distribution of λ_{PEAK} , as is expected from QDs suspended in an isotropic mixture. When cooled back into the CLC phase (25°C), another PL scan [Fig. 2(c)] shows that the associated λ_{PEAK} gradient has returned. While the emission wavelengths appear slightly blue shifted overall in Fig. 2(c), the pattern and directionality are similar to those observed in Fig. 2(a). The blue shift is most likely a result of photo-oxidation of the QDs under irradiation.²⁶ Photoluminescence intensity maps corresponding to each of the three experimental stages do not exhibit this stripe formation either in the CLC or the isotropic phase. However, from the clear similarities between the QD spectral emission patterns of Figs. 2(a) and 2(c) and the CLC defect texture of Fig. 1(d), it is obvious that there is a connection between the Grandjean steps and the measured QD PL emission stripes.

To understand this pattern formation, we make a spectral comparison of the CLC stop band and the QD emission in Fig. 3 in three samples prepared with different ratios of 5CB to COC to tune the pitch. Fig. 3(a) shows spectra for a sample prepared with 44 wt% 5CB to COC and a pitch of approximately 620 nm. Here, the peak emission of the QDs dispersed in the isotropic phase (circle) overlaps with

the short wavelength side of the CLC stop band (square), and the first observations we make are an overall red shift of the QD emission (triangle) and an increase in intensity when the sample is cooled into the cholesteric phase. A detailed analysis of the data reveals a more complicated behavior. It has been predicted that, due to the inherent dichroism, even in the isotropic phase a cholesteric system can modify optical transmission through it.²⁷ We notice the effects of such modifications in the following two ways: (a) although the QD emission in solution occurs at 608 nm, in the isotropic phase the emission has blue shifted and (b) the peak is not a Gaussian distribution but has a more asymmetric shape. To understand the latter, we perform a multipeak fit analysis using a standard nonlinear Levenberg-Marquardt algorithm where the peak positions and peak widths remain constant and only the relative amplitudes of the peaks are allowed to vary when fitting data from the same sample under different conditions. We find that both emissions (in the isotropic and CLC phases) are best explained as a cumulative effect of three subsets of QDs. These three consist of QDs emitting to the far left and completely outside, at the very edge, and completely inside the stop band (supplementary material, Fig. S1).²⁸ In the isotropic phase the emission is dominated by the subset that lies to the far left of the stop band while PL from those within the band is quenched, accounting for the asymmetric shape. When cooled to the CLC phase, the spectral weight shifts to the QDs emitting at the edge of the stop band, causing the spectrum to exhibit an overall red shift of 5 nm. The typical error in our fits λ_{PEAK} is ~ 0.5 nm.

Figure 3(b) plots the emission of the QDs (circle) from an arbitrary spot in the sample shown in Fig. 2 when it is in the isotropic phase. The multipeak protocol executed above is repeated and shows a similar result for this phase, with the emission again being dominated by the QDs that emit outside (but, this time, to the right) of the stop band (supplementary material, Fig. S2).²⁸ The spectrum though still blue shifted from the solution emission, is not as affected as in the previous sample. As the sample is cooled and the CLC phase forms, we observe that now the QD emission overlaps with the long wavelength edge of the CLC stop band. The QD spectrum from that same spot (triangle) is again predominantly from the QDs emitting at the edge of the stop band and, as a result, blue shifted by 3 nm, with the peak intensity greater than the peak intensity from QDs in the isotropic phase by a factor of 2. Figure 3(c) shows the stop band of a mixture of 20 wt% of 5CB to COC with a pitch of approximately 525 nm. The QD emission spectrum in the isotropic phase (circle) does not overlap with the stop band at all, and we now observe several points. First, the emission in the isotropic phase now occurs exactly at 608 nm, where the QDs emit in solution. Second, the distribution of spectral weight among different subsets of QDs is unchanged between the spectra obtained in the isotropic and the CLC phases (supplementary material, Fig. S3),²⁸ resulting in no discernible overall spectral shift. And, finally, there is a decrease in the emission intensity of the QDs (triangle) in the CLC phase compared to that in the isotropic solution. From these results shown in Fig. 3, it is clear that the spectral modification of the QD emission is caused by the optical confinement provided by the CLC and that the magnitude of this modification depends on the extent to which

the QD and CLC spectra overlap. When there is an overlap [Figs. 3(a) and 3(b)], the QD emission is amplified at the very edges of the stop band, resulting in a small spectral shift as the intensity weight redistributes. But when there is no overlap [Fig. 3(c)] there is no such enhancement. In Fig. 2 the QD emission lies near the long wavelength edge of the CLC stop band, similarly to that shown in Fig. 3(b), and as the stop band shifts toward the red with position from L to R, it continuously amplifies an increasingly redder portion of the QD spectrum, resulting in the observed pattern where the emission red shifts across a Grandjean step. When the pitch abruptly returns to its original value the QD emission pattern repeats itself.

We are effectively utilizing the CLC phase as a one-dimensional photonic band-gap material and tuning the emission of the ensemble of QDs by spatially altering the pitch of the CLC medium using the wedge cell. When the cholesteric helix is destroyed by raising the sample temperature above the isotropic phase transition [Fig. 2(b)], without a well-defined pitch to sustain a stop band, the QD emission randomizes. This stripe formation is thermally reversible and robust. The idea of emission amplification at the long-wavelength edge of the cholesteric reflection band has been employed previously to create a liquid crystal laser.^{29,30} The dyes used in these measurements have been rod-shaped molecules with emission linearly polarized along their long axis. This leads to multiple reflections and amplification of the emission that lies only near the long edge of the stop band. CdSe/ZnS QDs have a more isotropic emission compared to dyes, even when embedded

in nematic LC.^{17,31} The fact that the amplification is still observed, and occurs at both ends of the stop band, is surprising and suggestive of a more complicated modulation by the CLC medium than in the case of dyes.³²

To investigate the transmission of QD emission through the cholesteric phase in detail we have carried out further work to characterize the emission polarization of the QD-CLC sample. Figures 4(a) and 4(b) are spatially resolved PL maps showing the λ_{PEAK} variations over the same region of the sample but observed through a linear polarizer aligned vertically and horizontally, respectively. The horizontal direction, denoted $\theta = 0^\circ$ in our setup, is parallel to the rubbing direction of the Cano-wedge cells. Again, as before, a wavelength gradient is observed similar to that in Fig. 2. However, while Fig. 4(a) shows the gradient moving from longer to shorter wavelengths across the step, in Fig. 4(b) the gradient is reversed. In Fig. 4(c) we have plotted data along the lines indicated in Figs. 4(a) and 4(b), where we see the sawtooth pattern of the QD peak emission, and that the horizontally ($\theta = 0^\circ$) and vertically ($\theta = 90^\circ$) polarized components are essentially reversed. The corresponding spectrally integrated intensity maps display neither stripes nor any clear difference between the two polarization configurations, although it is interesting to note that the data collected without polarization optics in Figs. 2(a) and 2(c) resembles the pattern in Fig. 4(b), implying the emission intensity along that 0° is slightly larger than that observed along 90° . We attribute this to the fact that 0° is aligned along the rubbing direction which defines the director of the nematic component (5CB) in the CLC composite. Emission intensity is typically greater along that direction due to reduced scattering irrespective of any other effect (supplementary material, Fig. S4).²⁸

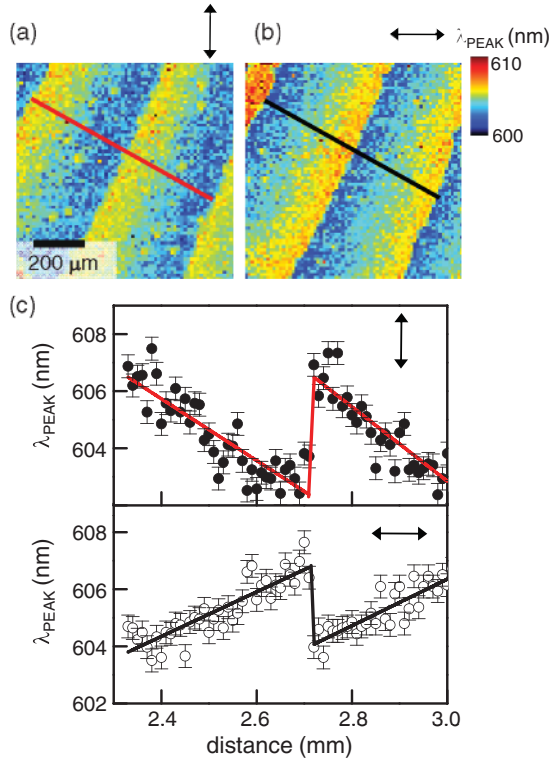


FIG. 4. (Color online) Polarization resolved PL maps of λ_{PEAK} when observed (a) perpendicular (90°) and (b) parallel (0°) to the rubbing direction. (c) Plot of λ_{PEAK} for (a) and (b) along the lines shown on the maps. λ_{PEAK} of (a) are plotted as solid circles (top) and (b) as open circles (bottom). Lines are linear fits to data.

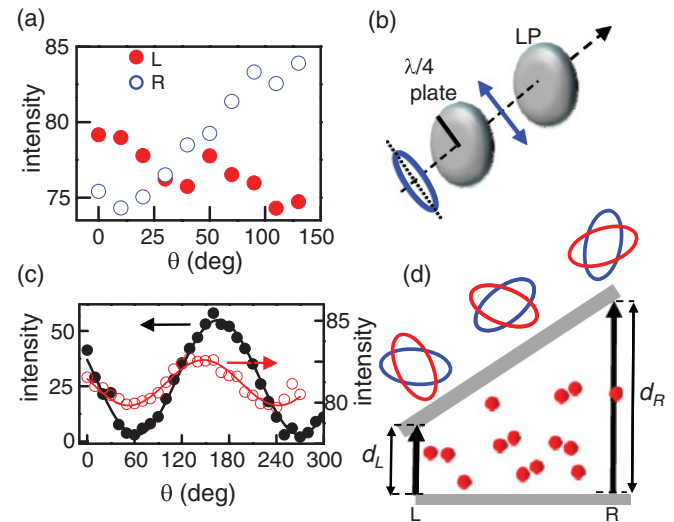


FIG. 5. (Color online) (a) PL emission varying with the angle with respect to the rubbing direction, θ , at the two edges (L and R) of one step. (b) Schematic of optical path used to analyze emission polarization using a combination of a quarter wave ($\lambda/4$) plate and a linear polarizer (LP). (c) Polarization resolved PL intensity as a function of angle θ between the rubbing direction and the LP with (solid circles) and without (open circles) the $\lambda/4$ plate. (d) Schematic depicting the QD emission polarization states changing across the Grandjean steps with increasing path difference d .

To investigate the polarization dependence further, we track the spectrally discrete peak intensities of QD emission for two spots at the beginning and end of a Grandjean step, as a function of θ , shown in Fig. 5(a). Here we observed that the peak intensity at the beginning of a step (marked “L”) is highest when the polarizer is aligned along the rubbing direction and decreases with increasing θ . At the same time, the intensity at the end of the edge (marked “R”) is initially small but increases with θ . Together with the differences between Figs. 4(a) and 4(b), these results suggest that as the emission from the left edge of a step red-shifts between the 0° and 90° directions, the intensity simultaneously decreases. The exact reverse occurs at the right edge. These variations are small (on the order of 6–10%) but systematic. To confirm the effect, a more detailed measurement of QD PL intensity from an arbitrary region is carried out. Shown in Fig. 5(c) (open circles) we see that although the emission intensity exhibits a sinusoidal variation with θ , the signal does not fall to zero at any angular position of the linear polarizer. This is a surprising result because it is generally assumed that the emission from a cholesteric device should be circularly polarized following the helicity of the CLC.³³ Our results clearly demonstrate that the transmitted PL is not circularly polarized (in which case there should be zero or negligible variation in intensity with θ) but is partially linearly polarized, elliptically polarized, or a mixture of the two. To determine which, we insert a $\lambda/4$ plate before the linear polarizer in the collection path [Fig. 5(b)], with the fast axis of the $\lambda/4$ plate aligned along the direction of maximum transmission, which in our case is 145° [Fig. 5(c), open circles]. Then we rotate the linear polarizer again and plot the resulting intensity as a function of θ in Fig. 5(c) (solid circles). Now we can clearly observe that the resultant intensity does go to zero, although the maximum occurs at a different angle. This is a definite indication that the emission is elliptically polarized. We can approximate that the ellipse major axis is tilted by 35° to the rubbing direction, where the emission intensity was maximized prior to inserting the $\lambda/4$ plate.

This confirmation of elliptically polarized emission implies the CLC medium is exhibiting circular dichroism in addition to the expected circular birefringence and that it imparts an arbitrary phase to the electromagnetic radiation traveling through it. This phase δ is given by $\delta = (\pi \Delta n/\lambda)d$, where d is the path length through the sample and Δn is the difference in refractive indices as is typical of a birefringent material.³⁴ For elliptically polarized light the tilt of the ellipse is a function of δ , and since δ is dependent of the wavelength λ , it follows that the different parts of the QD PL spectrum will be polarized at slightly different angles to the rubbing direction. This allows us to come up with a simple pictorial representation as shown

in Fig. 5(d). At the beginning of a Grandjean step at “L” $d_L = p$, and from the data in Figs. 4(a) and 4(b), this appears to satisfy the condition where the shortest wavelength of the QD emission is polarized with the major axis closer to the horizontal direction with reference to our measurement scheme. The other “colors” form ellipses titled along different angles, ending with the longest wavelength closest to the 90° axis. Moving across the step, d changes until at the end of a step at R $d_R \rightarrow 3p/2$. Using typical values of Δn in CLC materials,³⁵ this corresponds to a negligible phase difference between points L and R. However, in a confined geometry the reflection-induced multiple passes through the CLC medium enhances the phase difference greatly. A simple approximation for our system gives us an estimate of a photon confinement time $\sim 10^{-13}$ s, which translates to about 25 passes. In turn, this implies a total phase difference 25 times bigger than the previously calculated δ , which would lead to a considerable reorientation of the emission ellipses between L to R (as shown by the blue and red ellipses). This explains why we observe the complimentary spectral maps when viewed along 0° and 90° .

IV. CONCLUSIONS

We have demonstrated the fabrication of a QD embedded one-dimensional photonic cavity constructed from a cholesteric liquid crystal. The liquid crystal medium selectively enhances the PL from a subset of QDs whose emission spectrally overlaps with the edges of the stop band. The mechanism of such amplification is most likely due to the Purcell effect³⁶ as preliminary time-resolved data show an increase in the recombination rates in the QD-CLC samples when compared to the recombination rates of the QDs in solution. However, unlike typical photonic band gap materials, such as naturally occurring crystalline solids³⁷ or those fabricated from semiconducting structures,³⁸ the stop band of the CLC can be easily tuned by altering the ratio of its components and additionally externally modulated using temperature or electric fields. This greatly enhances the spectral flexibility of the photonic device. The controllable spatial variation in spectral emission and polarization that is imparted by the CLC medium provides excellent possibilities for increased device functionality, making this liquid crystal matrix a very attractive platform for designing new QD-based optical materials.

ACKNOWLEDGMENTS

The authors acknowledge funding from UC MEXUS and UC MERI.

*lhirst@ucmerced.edu

†sghosh@ucmerced.edu

¹T. Hegmann, H. Qi, and V. M. Marx, *J. Inorg. Organomet. Polym. Mater.* **17**, 483 (2007).

²R. W. Ruhwandl and E. M. Terentjev, *Phys. Rev. E* **55**, 2958 (1997).

³S. P. Meeker, W. C. K. Poon, J. Crain, and E. M. Terentjev, *Phys. Rev. E* **61**, R6083 (2000).

⁴P. Poulin, H. Stark, T. C. Lubensky, and D. A. Weitz, *Science* **275**, 1770 (1997).

⁵M. D. Lynch and D. L. Patrick, *Nano Lett.* **2**, 1197 (2002).

⁶I. Dierking, G. Scalia, and P. Morales, *J. Appl. Phys.* **97**, 044309 (2005).

⁷C. Pizzey, S. Klein, E. Leach, J. S. van Duijneveldt, and R. M. Richardson, *J. Phys. Condens. Matter* **16**, 2479 (2004).

- ⁸M. Kawasumi, A. Usuki, A. Okada, and T. Kurauchi, *Mol. Cryst. Liq. Cryst.* **281**, 91 (1996).
- ⁹M. P. VanBruggen, F. M. VanderKooij, and H. N. W. Lekkerkerker, *J. Phys. Condens. Matter* **8**, 9451 (1996).
- ¹⁰C. P. Lapointe, T. G. Mason, and I. I. Smalyukh, *Science* **326**, 1083 (2009).
- ¹¹L. S. Hirst, J. Kirchoff, R. Inman, and S. Ghosh, *Proc. SPIE* **7618**, 76180F (2010).
- ¹²R. Bitar, G. Agez, and M. Mitov, *Soft Matter* **7**, 8198 (2011).
- ¹³Y. Shiraishi, N. Toshima, K. Maeda, H. Yoshikawa, J. Xu, and S. Kobayashi, *App. Phys. Lett.* **81**, 2845 (2002).
- ¹⁴B. Kinkead and T. Hegmann, *J. Mater. Chem.* **20**, 448 (2010).
- ¹⁵U. Tkalec, M. Ravnik, S. Copar, S. Zumer, and I. Muševic, *Science* **333**, 62 (2011).
- ¹⁶H. Yoshida, Y. Tanaka, K. Kawamoto, H. Kubo, T. Tsuda, A. Fujii, S. Kuwabata, H. Kikuchi, and M. Ozaki, *Appl. Phys. Express* **2**, 21501 (2009).
- ¹⁷Y. K. Verma, R. H. Inman, C. G. L. Ferri, H. Mirafzal, S. N. Ghosh, D. F. Kelley, L. S. Hirst, S. Ghosh, and W. C. Chin, *Phys. Rev. B* **82**, 165428 (2010).
- ¹⁸P. Borri, W. Langbein, J. M. Hvam, F. Heinrichsdorff, M.-H. Mao, and D. Bimberg, *IEEE Photonics Technol. Lett.* **12**, 594 (2000).
- ¹⁹S. Chang, M. Zhou, and C. P. Grover, *Opt. Exp.* **12**, 143 (2004).
- ²⁰D. Loss and D. P. DiVincenzo, *Phys. Rev. A* **57**, 120 (1998).
- ²¹P. J. Collings, *Liquid Crystals: Nature's Delicate Phase of Matter* (Princeton University Press, Princeton, NJ, 2002).
- ²²H. L. De Vries, *Acta. Crystallogr.* **4**, 219 (1951).
- ²³S. M. Feng and T. Chen, *Displays* **30**, 195 (2009).
- ²⁴F. Grandjean, *C. R. Acad. Sci.* **172**, 71 (1921).
- ²⁵D. Podolsky, O. Banji and P. Rudquist, *Liq. Cryst.* **35**, 789 (2008).
- ²⁶M. Jones, J. Nedeljkovic, R. J. Ellingson, A. J. Nozik, and G. Rumbles, *J. Phys. Chem. B* **107**, 11346 (2003).
- ²⁷Julian Cheng and Robert B. Meyer, *Phys. Rev. A* **9**, 2744 (1974).
- ²⁸See Supplemental Material at <http://link.aps.org/supplemental/10.1103/PhysRevB.85.035430> for results of the multipeak fitting.
- ²⁹V. I. Kopp, B. Fan, H. K. M. Vithana, and A. Z. Genack, *Opt. Lett.* **23**, 1707 (1998).
- ³⁰B. Taheri, A. F. Munoz, P. Palfy-muhoray, and R. Twieg, *Mol. Cryst. Liq. Cryst.* **358**, 73 (2001).
- ³¹J. Hu, L.-S. Li, W. Yang, L. Manna, L.-W. Wang, and A. P. Alivisatos, *Science* **292**, 2060 (2001).
- ³²M.-Y. Jeong, H. Choi, and J. W. Wu, *Appl. Phys. Lett.* **92**, 051108 (2008).
- ³³S. G. Lukishova, L. J. Bissell, C. R. Stroud Jr., and R. W. Boyd, *Opt. Spectrosc.* **108**, 417 (2010).
- ³⁴P. J. Collings and M. Hird, *Introduction to Liquid Crystals: Chemistry and Physics* (Taylor & Francis, Philadelphia, 2004).
- ³⁵P. Yeh and C. Gu, *Optics of Liquid Crystal Displays* (John Wiley & Sons, Inc., Hoboken, 2010).
- ³⁶E. M. Purcell, *Phys. Rev.* **69**, 681 (1946).
- ³⁷J. D. Joannopoulos, S. G. Johnson, J. N. Winn and R. D. Meade, *Photonic Crystals: Molding the Flow of Light*, 2nd ed. (Princeton University Press, Princeton, NJ, 2008).
- ³⁸S. Strauf *et al.*, *Appl. Phys. Lett.* **88**, 043116 (2006).